Propagation characteristics of ultrawide-bandwidth pulsed Gaussian beams

Richard W. Ziolkowski and Justin B. Judkins

Department of Electrical and Computer Engineering, University of Arizona, Tucson, Arizona 85721

Received January 21, 1992; revised manuscript received May 20, 1992; accepted May 28, 1992

The propagation characteristics of a beam generated by driving an aperture with an ultrashort, hence ultrawide-bandwidth, space–time Gaussian pulse are considered. It is shown analytically with an approximate form of the solution that the beam intensity and the beam energy have different diffraction lengths and rates of beam spread in the far field. These beam properties are also discussed for a derivative receiver system. The analytical results are supported with numerical simulations of the exact pulsed-beam solution.

1. INTRODUCTION

As modern science expands its horizons in the development of stable, repeatable pulsed sources of signals in the 10^{-12}- to 10^{-15}-s regimes, we are quickly approaching the realization of electromagnetic energy devices and their applications in those regimes. The need for understanding the characteristics of the beams generated by these millimeter-wave and optical pulsed sources is important for the successful engineering of those applications. Most conventional sources can be classified as being cw (monochromatic) or having narrow bandwidths (being quasi-monochromatic). The characteristics of the Gaussian beams resulting from these sources are well known and can be found in a variety of textbooks.[1,2] However, as the bandwidths of the pulses increase, their properties can no longer be characterized by those cw results. The purpose of this paper is to derive and characterize the beam generated by sources of ultrashort (time-limited), hence ultrawide-frequency-bandwidth, pulses. Comparisons with the results predicted for general systems of this type[3] are made.

The propagation characteristics of the beam generated by driving an aperture with an ultrashort, time-limited (hence ultrawide-frequency-bandwidth) signal whose amplitude is weighted as a Gaussian across the aperture are derived in Section 2. Particular attention is given to the case involving a Gaussian time signal. An approximate form of the resulting pulsed Gaussian beam field is derived in Section 3. It is shown that the beam intensity and the beam energy have different diffraction lengths and rates of beam spread in the far field. Similar properties are derived in Section 4 for a pulsed Gaussian beam measured with a derivative detector. The conclusions of Sections 3 and 4 are supported with numerical simulations as described in Section 5. In particular, the spatial and temporal behaviors of a femtosecond pulsed Gaussian beam are studied. A summary and suggestions for experimental confirmation of these results are given in Section 6.

2. PULSED GAUSSIAN BEAM FIELD

Consider a circular aperture of radius a in the plane $z = 0$. We assume that this aperture is driven everywhere with the Gaussian time signal

$$F(t) = \exp(-pt^2). \tag{1}$$

The field is assumed to propagate from the initial aperture into the half-space $z > 0$, which is taken to be a dispersionless, lossless, linear medium. To simplify the analysis, we assume that the radius of the aperture is sufficiently larger than the waist w_0 of this initial pulse to remove any edge effects from the discussion.

Since the system is linear, this initial field will evolve into a pulsed electromagnetic Gaussian beam that is propagating in free space. We can thus use standard linear-system theory and known representations for a cw Gaussian beam to derive an expression for the resulting pulsed beam in the desired half-space. In particular, we use the well-known frequency-domain representation of the amplitude of a linearly polarized electric field (polarized in a direction orthogonal to the direction of propagation) of an azimuthally symmetric, zeroth-order, Gaussian beam in a homogeneous medium. If the propagation direction is assumed to be along the z axis, this field has the form[1]

$$\tilde{E}(r,\phi,z,\omega) = E_0 \frac{\omega_0}{\omega(z)} \exp\left\{-i[kz - \eta(z)] - r^2\left[\frac{1}{w^2(z)} + \frac{ik}{2R(z)}\right]\right\}, \tag{2}$$

where the waist, the radius of curvature, the phase term, and the diffraction length, respectively, are given by

$$w^2(z) = w_0^2\left[1 + \left(\frac{\lambda z}{\pi w_0^2}\right)^2\right] = w_0^2\left(1 + \frac{z^2}{z_0^2}\right), \tag{3}$$

$$R(z) = z\left[1 + \left(\frac{\pi w_0^2}{\lambda z}\right)^2\right] = z\left(1 + \frac{z_0^2}{z^2}\right), \tag{4}$$

$$\eta(z) = \tan^{-1}\left(\frac{\lambda z}{\pi w_0^2}\right) = \tan^{-1}\left(\frac{z}{z_0}\right), \tag{5}$$

$$z_0 \equiv \frac{\pi w_0^2}{\lambda} = \left(\frac{w_0^2}{2c}\right)\omega. \tag{6}$$

0740-3232/92/112021-10$05.00

The rate of beam spread (beam-spread angle) in the far field where $z \gg z_0$ follows from the waist expression [Eq. (4)]:

$$\theta_{cw} = \tan^{-1}\left[\frac{w(z)}{\sqrt{2}z}\right] \approx \tan^{-1}\left(\frac{\lambda}{\sqrt{2}\pi w_0}\right) \approx \sqrt{2}\left(\frac{\lambda}{2\pi w_0}\right). \tag{7}$$

Instead of taking the usual definition of θ_{cw} as the radius at which the amplitude has decreased to $1/e$ of its value on the axis, we have defined this angle to be the radius at which the intensity has decreased to $1/e$ of its value on the axis. Note that the same angle would have been obtained from the energy profile in this cw case. The usual definition results in relation (7) without the $1/\sqrt{2}$ factor.

When the driving function has a Gaussian time history, it also has a Gaussian spectrum. In particular, the temporal Fourier transform of the initial pulse given by Eq. (1) is

$$\tilde{F}(\omega) = (\pi/p)^{1/2} \exp(-\omega^2/4p). \tag{8}$$

Therefore the resulting beam field in the region $z > 0$ is the inverse Fourier transform of the product of the spectral fields given by Eqs. (2) and (8):

$$E(r,\phi,z,t) = \frac{1}{2\pi}\int_{-\infty}^{\infty} \tilde{E}(r,\phi,z,\omega)\tilde{F}(\omega)\exp(+i\omega t)\mathrm{d}\omega. \tag{9}$$

The intensity of the beam at the field point (r,ϕ,z) is determined by squaring the electric field given by Eq. (9); the energy is obtained by integrating the intensity over all time. This discussion is extended in a straightforward manner to Gaussian beam modes of any order and symmetry.

3. ANALYTICAL CHARACTERIZATION OF PULSED GAUSSIAN BEAMS

An approximate form of the field expression [Eq. (2)] is readily obtained, so that a similar form can be derived from Eq. (9) analytically. When $z \ll z_0$, one has from Eq. (3) that the waist $w(z) \simeq w_0$. The approximation for the electric field at an observation point near the initial surface for a particular angular frequency ω then becomes

$$\tilde{E}(r,\phi,z,\omega) \approx E_0 \exp(-ikz)\exp(-r^2/w_0^2) \qquad (z \ll z_0). \tag{10}$$

Thus the cw beam retains essentially a Gaussian shape in any transverse plane; its amplitude remains constant along the z axis. However, as the distance away from the aperture increases, the waist given by Eq. (3) becomes more dependent on z. In fact, for $z \gg z_0$ Eq. (3) becomes

$$w(z) \simeq w_0(z/z_0), \tag{11}$$

and the resulting approximation for the frequency domain field far away from the initial $z = 0$ plane is

$$\begin{aligned}\tilde{E}(r,\phi,z,\omega) &\approx E_0\frac{z_0}{z}\exp\left\{-i\left(kz-\frac{\pi}{2}\right) - r^2\left[\left(\frac{z_0}{w_0 z}\right)^2 + \frac{ik}{2z}\right]\right\} \\ &= iE_0\frac{w_0^2}{2cz}\omega\exp\left[-i\omega\left(\frac{z}{c}+\frac{r^2}{2cz}\right) - \omega^2\left(\frac{w_0 r}{2cz}\right)^2\right] \\ &\qquad (z \gg z_0). \end{aligned} \tag{12}$$

Although an analytical expression for Eq. (9) is not directly available, it can be reasonably approximated by using Eq. (8) and relations (10) and (12) and performing the inverse transforms analytically. With Eq. (3.323.2) of Ref. 4, one obtains

$$E(r,\phi,z,t) \approx E_0 \exp(-r^2/w_0^2)\exp[-p(z/c - t)^2] \tag{13}$$

near the aperture and

$$\begin{aligned} &E(r,\phi,z,t) \\ &\approx \frac{E_0}{2\pi}\left(\frac{\pi}{p}\right)^{1/2}\frac{w_0^2}{2cz}\int_{-\infty}^{\infty} i\omega\exp\left\{-\omega^2\left[\frac{1}{4p}+\left(\frac{w_0 r}{2cz}\right)^2\right]\right\} \\ &\quad\times\exp\left\{-i\omega\left[\left(\frac{z}{c}-t\right)+\frac{r^2}{2cz}\right]\right\}\mathrm{d}\omega \\ &= \frac{E_0}{2\pi}\left(\frac{\pi}{p}\right)^{1/2}\frac{w_0^2}{2cz}\partial_t\left(\int_{-\infty}^{\infty}\exp\left\{-\omega^2\left[\frac{1}{4p}+\left(\frac{w_0 r}{2cz}\right)^2\right]\right\}\right. \\ &\quad\left.\times\exp\left\{-i\omega\left[\left(\frac{z}{c}-t\right)+\frac{r^2}{2cz}\right]\right\}\mathrm{d}\omega\right) \\ &= E_0\frac{pw_0^2}{cz}\left[\frac{1}{1+p(w_0 r/cz)^2}\right]^{3/2}\left(\frac{z}{c}-t+\frac{r^2}{2cz}\right) \\ &\quad\times\exp\left[-p\frac{(z/c-t+r^2/2cz)^2}{1+p(w_0 r/cz)^2}\right] \end{aligned} \tag{14}$$

far from the aperture. Thus the initial pulsed beam retains its form near the aperture and acquires a time-derivative form that decays as z^{-1} far from it. The specification of the diffraction length of this field (distance to the near- to far-field boundary) is given below.

The time-derivative behavior far from the aperture represented by relation (14) is expected from the radiation process. Recall that the field away from the aperture can be treated as arising from a set of equivalent electric and magnetic sources in the aperture; i.e., if $\hat{\mathbf{n}}_{ap}$ is the normal to the aperture in the direction of propagation, the equivalent (dipole) current sources in the aperture may be formed from the tangential electric and magnetic fields there: $\mathbf{J}_{ap} = \hat{\mathbf{n}} \times \mathbf{H}_{ap}$ and $\mathbf{M}_{ap} = -\hat{\mathbf{n}} \times \mathbf{E}_{ap}$. In the near field close to the aperture, rather than being dominated by the individual dipole sources, the electromagnetic field is dominated by the induction fields of these current sources, and those fields are directly related to the tangential electric and magnetic fields in the aperture, so that $\mathbf{E}_{near} \propto \mathbf{E}_{ap}$ and $\mathbf{H}_{near} \propto \mathbf{H}_{ap}$. One then expects, as shown above, that the initial field will be recovered near the aperture, modulo a phase term. The radiated (far-field) electric field can be simply connected to the aperture field; it is related to a time derivative of the electric vector potential, which in turn is proportional to the aperture electric-current density: $\mathbf{E}_{far} \propto -\partial_t \mathbf{A}_e \propto \partial_t \mathbf{J}_{ap}$. However, the fields in and near the aperture are dominated by the TEM-like property that they are nearly translationally invariant along the propagation direction. This means that $\partial_{ct} Z_0 \mathbf{H}_{near} \sim \partial_z(\hat{\mathbf{n}}_{ap} \times \mathbf{E}_{near})$ and hence $Z_0 \mathbf{H}_{near} \sim \hat{\mathbf{n}}_{ap} \times \mathbf{E}_{near}$, so that $\mathbf{J}_{ap} \propto \mathbf{H}_{ap} \propto \mathbf{E}_{ap}$. These near- and far-field arguments then give $\mathbf{E}_{far} \propto \partial_t \mathbf{E}_{ap}$. Thus as the field evolves from the near- to the far-field region, it acquires the observed time-derivative behavior.

The intensity of the beam field in the near- and far-field regions is readily obtained as the absolute square of the

electric fields given by relations (13) and (14). One obtains for the near field

$$\mathcal{I}(r,\phi,z,t) \approx |E(r,\phi,z,t)|^2 = |E_0|^2 \exp(-2r^2/w_0^2)\exp[-2p(z/c - t)^2] \quad (15)$$

and for the far field

$$\mathcal{I}(r,\phi,z,t) \approx E_0^2\left(\frac{pw_0^2}{cz}\right)^2\left[\frac{1}{1 + p(w_0 r/cz)^2}\right]^3\left(\frac{z}{c} - t + \frac{r^2}{2cz}\right)^2 \times \exp\left[-2p\frac{(z/c - t + r^2/2cz)^2}{1 + p(w_0 r/cz)^2}\right]. \quad (16)$$

Because the intensity depends on time, it has limited usefulness as a cogent beam quantity. A more descriptive quantity is the maximum of the intensity in time: $\mathcal{I}_{\max} = \max_t \mathcal{I}$. It allows one to associate a pattern (transverse spatial distribution) with the intensity. Setting the partial with respect to time of the electric fields given by relations (13) and (14) to zero, one finds that the maxima of the electric field are located at the time $t_{\max} = z/c$ in the near field and at the time

$$t_{\max} = \frac{z}{c} + \frac{r^2}{2cz} \pm \left(\frac{1}{2p} + \frac{w_0^2 r^2}{2c^2 z^2}\right)^{1/2} \quad (17)$$

in the far field, so that the maximum intensity received at an observation point is

$$\mathcal{I}_{\max}(r,\phi,z) = E_0^2 \exp(-2r^2/w_0^2) \quad (18)$$

in the near field and

$$\mathcal{I}_{\max}(r,\phi,z) \approx \frac{1}{2e}E_0^2\left(\frac{w_0^2}{cz}\right)^2 p\left[1 + p\left(\frac{w_0 r}{cz}\right)^2\right]^{-2} \quad (19)$$

in the far field. Consequently, the ratio of the maximum intensity along the axis of propagation to the maximum intensity on axis at the aperture $z = 0$ is

$$\Gamma_{\text{int},\parallel}(r = 0,\phi,z) \overset{\text{def}}{=} \frac{\mathcal{I}_{\max}(r = 0,\phi,z)}{\mathcal{I}_{\max}(r = 0,\phi,z = 0)} = \begin{cases} 1.0 & \text{(near field)} \\ \dfrac{p}{2e}\left(\dfrac{w_0^2}{zc}\right)^2 & \text{(far field)} \end{cases}. \quad (20)$$

Similarly, the ratio of the maximum intensity at a point in a plane orthogonal to the axis of propagation to its value on that axis will be

$$\Gamma_{\text{int},\perp}(r,\phi,z) = \frac{\mathcal{I}_{\max}(r,\phi,z)}{\mathcal{I}_{\max}(r = 0,\phi,z)} = \begin{cases} \exp(-2r^2/w_0^2) & \text{(near field)} \\ \left(1 + p\dfrac{w_0^2 r^2}{c^2 z^2}\right)^{-2} & \text{(far field)} \end{cases}. \quad (21)$$

The maximum-intensity profile remains the same in the near field but begins to spread in the far field. One can thus define a beam spread in the far field for the maximum intensity θ_{int} in terms of the far-field ratio [Eq. (21)]. In particular, let R_{int} be the value of ratio (21) in the far field at which the beam spread is taken. With this quantity one then has

$$\theta_{\text{int}} \overset{\text{def}}{=} \frac{r}{z} = \left[(R_{\text{int}}^{-1/2} - 1)\frac{c^2}{pw_0^2}\right]^{1/2}. \quad (22)$$

A standard choice of the evaluation point of the beam spread ratio would be the $1/e$ point, i.e., taking $R_{\text{int}} = 1/e$.

On the other hand, the energy at a field point (r,ϕ,z) is determined simply by integrating the intensities given by relations (15) and (16) over all time. With Eqs. (3.463.6) and (3.463.8) of Ref. 4, one obtains

$$\mathcal{E}(r,\phi,z) \approx \int_{-\infty}^{\infty} |E_0|^2 \exp(-2r^2/w_0^2)\exp[-2p(z/c - t)^2]dt = |E_0|^2 \exp(-2r^2/w_0^2)\left(\frac{\pi}{2p}\right)^{1/2} \quad (23)$$

in the near field and

$$\mathcal{E}(r,\phi,z) \approx \frac{E_0^2[pw_0^2/(cz)]^2}{\{1 + p[w_0 r/(cz)]^2\}^3}\int_{-\infty}^{\infty}\left(\frac{z}{c} - t + \frac{r^2}{2cz}\right)^2 \times \exp\left[-2p\frac{(z/c - t + r^2/2cz)^2}{1 + p(w_0 r/cz)^2}\right]dt = E_0^2\left(\frac{w_0^2}{2cz}\right)^2\left(\frac{\pi}{2}p\right)^{1/2}\left[1 + p\left(\frac{w_0 r}{cz}\right)^2\right]^{-3/2} \quad (24)$$

in the far field. Consequently, the ratio of the energy along the axis of propagation to the energy on axis at the aperture $z = 0$ is

$$\Gamma_{\text{enrg},\parallel}(r = 0,\phi,z) \overset{\text{def}}{=} \frac{\mathcal{E}(r = 0,\phi,z)}{\mathcal{E}(r = 0,\phi,z = 0)} = \begin{cases} 1.0 & \text{(near field)} \\ p(w_0^2/2cz)^2 & \text{(far field)} \end{cases}. \quad (25)$$

Similarly, the ratio of the energy at a point in a plane orthogonal to the axis of propagation to its value on that axis is

$$\Gamma_{\text{enrg},\perp}(r,\phi,z) = \frac{\mathcal{E}(r,\phi,z)}{\mathcal{E}(r = 0,\phi,z)} = \begin{cases} \exp(-2r^2/w_0^2) & \text{(near field)} \\ [1 + p(w_0^2 r^2/c^2 z^2)]^{-3/2} & \text{(far field)} \end{cases}. \quad (26)$$

The energy profile remains the same in the near field but begins to spread in the far field. One can thus define a beam spread in the far field for the energy θ_{enrg} in terms of the far-field ratio [Eq. (26)]. In particular, let R_{enrg} be the value of ratio (26) in the far field at which the beam spread is taken. With this quantity one then has

$$\theta_{\text{enrg}} \overset{\text{def}}{=} \frac{r}{z} = \left[(R_{\text{enrg}}^{-2/3} - 1)\frac{c^2}{pw_0^2}\right]^{1/2}. \quad (27)$$

A standard choice of the evaluation point of the beam-spread ratio would again be the $1/e$ point, i.e., taking $R_{\text{enrg}} = 1/e$.

Now we would like to characterize the far-field maximum intensity and energy in terms of the effective

frequency associated with the radiated field that was introduced in Ref. 3. This effective frequency was obtained from analytical bounds on the rate of energy decay along the direction of propagation of the beam generated by an arbitrary array driven with a general spatially distributed set of time signals $\mathcal{F}(\mathbf{r}, t)$, by taking into account the time-derivative effect that results from the propagation of the beam from the near to the far field. For the case under consideration the initial time-signal distribution is $\mathcal{F}(\mathbf{r}, t) = E_0 \exp(-r^2/w_0^2)F(t)$, and the associated effective frequency is defined as

$$\omega_{\text{rad}}^2 \stackrel{\text{def}}{=} \frac{\int_A dS \int_{-\infty}^{\infty} dt |\partial_t \mathcal{F}(\mathbf{r}, t)|^2}{\int_A dS \int_{-\infty}^{\infty} dt |\mathcal{F}(\mathbf{r}, t)|^2} = \frac{\int_{-\infty}^{\infty} dt |\partial_t F(t)|^2}{\int_{-\infty}^{\infty} dt |F(t)|^2} = p. \quad (28)$$

This effective frequency ω_{rad} is a measure of the spectral energies radiated into the medium in our model. It is a ratio of the aperture-weighted accumulation of the contributions to the energy spectrum of the field away from the aperture to the aperture-weighted accumulation of the energy spectra of the signals driven into the aperture. It is a useful quantity since it characterizes by a single frequency value all the ultrawide-bandwidth components contained in all the signals radiated by the aperture. We now rewrite the far-field intensity and energy relations in terms of this effective frequency ω_{rad}, its corresponding wavelength λ_{rad}, and the associated diffraction length L_{rad}:

$$\lambda_{\text{rad}} = \frac{2\pi c}{\omega_{\text{rad}}} = \frac{2\pi c}{\sqrt{p}}, \quad (28')$$

$$L_{\text{rad}} = \frac{\pi w_0^2}{\lambda_{\text{rad}}}. \quad (29)$$

In particular, one finds in the far field

$$\Gamma_{\text{int},\parallel}(r = 0, \phi, z) = \frac{2}{e}\left(\frac{\pi w_0^2}{\lambda_{\text{rad}} z}\right)^2 = \frac{2}{e}\left(\frac{L_{\text{rad}}}{z}\right)^2 \equiv \left(\frac{L_{\text{int}}}{z}\right)^2, \quad (20')$$

$$\theta_{\text{int}} = (R_{\text{int}}^{-1/2} - 1)^{1/2} \frac{\lambda_{\text{rad}}}{2\pi w_0}, \quad (22')$$

$$\Gamma_{\text{enrg},\parallel}(r = 0, \phi, z) = \left(\frac{\pi w_0^2}{\lambda_{\text{rad}} z}\right)^2 = \left(\frac{L_{\text{rad}}}{z}\right)^2 \equiv \left(\frac{L_{\text{enrg}}}{z}\right)^2, \quad (25')$$

$$\theta_{\text{enrg}} = (R_{\text{enrg}}^{-2/3} - 1)^{1/2} \frac{\lambda_{\text{rad}}}{2\pi w_0}. \quad (27')$$

Thus one readily observes that the diffraction lengths and the rate of beam spreading in the far field for the maximum intensity are different from those of the energy. Quantitatively, the diffraction lengths for the maximum intensity and maximum energy satisfy

$$\frac{L_{\text{int}}}{L_{\text{enrg}}} = \left(\frac{2}{e}\right)^{1/2} = 0.858, \quad (30)$$

and the rates of beam spread, by taking the $1/e$ roll-off point, satisfy

$$\frac{\theta_{\text{int}}}{\theta_{\text{enrg}}} = \left(\frac{R_{\text{int}}^{-1/2} - 1}{R_{\text{enrg}}^{-2/3} - 1}\right)^{1/2} = 0.827. \quad (31)$$

Although the diffraction lengths for maximum intensity are only slightly different from those for maximum energy, the rates of spreading of the intensity and the energy in the far field are significantly different, particularly if we consider the spot-size ramifications at large distances from the aperture. The differences, as explained in Ref. 3, result from the facts that the maximum intensity is a point quantity that depends on the bandwidth and the energy is an average quantity that hence depends on an average frequency value. We also note that, if the aperture were driven with a cw signal corresponding to the effective frequency $\omega_{\text{cw}} = \omega_{\text{rad}}$, a comparison of relation (7) with Eqs. (22′) and (27′) reveals that the ultrawide-bandwidth beam has energy and intensity profiles in the far field that are narrower than those of the cw case, e.g., $\theta_{\text{int}}/\theta_{\text{cw}} = [(e^{+1/2} - 1)/2]^{1/2} = 0.570$. Situations in which these differences could be designed to be much larger than they are in this simple but important example are discussed in Ref. 3.

The beam-energy decay and the beam-spread rate results are in excellent agreement with those predicted in Ref. 3 for such an ultrawide-bandwidth system. The intensity ratio can be put into the form suggested there with the introduction of the term

$$\Upsilon_{\text{rad}} \stackrel{\text{def}}{=} \frac{\max_t \int_A dS' |\partial_t F(\mathbf{r}', t)|^2}{\int_A dS' \int_{-\infty}^{\infty} dt |\partial_t F(\mathbf{r}', t)|^2} = \frac{4}{e}\left(\frac{p}{2\pi}\right)^{1/2} = \frac{2\sqrt{2}}{e\sqrt{\pi}}\omega_{\text{rad}}, \quad (32)$$

which is simply the ratio of the maximum of the aperture-weighted driving function to its time-averaged value. In particular, we can write the far-field maximum field intensity normalized by the product of the effective frequency, which characterizes the frequencies radiated from the aperture, and the energy (fluence) on axis at the aperture $z = 0$ as

$$\tilde{\Gamma}_{\text{int},\parallel}(r = 0, \phi, z) \stackrel{\text{def}}{=} \frac{\mathcal{I}_{\max}(r = 0, \phi, z)}{\omega_{\text{rad}} \mathcal{E}(r = 0, \phi, z = 0)} = \frac{2\sqrt{2}}{e\sqrt{\pi}}\left(\frac{\pi w_0^2}{\lambda_{\text{rad}} z}\right)^2 \equiv \frac{\Upsilon_{\text{rad}}}{\omega_{\text{rad}}}\left(\frac{L_{\text{rad}}}{z}\right)^2, \quad (33)$$

which coincides exactly with the behavior anticipated in Ref. 3.

4. PULSED GAUSSIAN BEAM MEASURED WITH A DERIVATIVE DETECTOR

Because a component signal of the pulsed Gaussian beam has a broad bandwidth, a receiver, which has its own natural-frequency set, can affect the measurement of this signal. On the other hand, since the signals are time limited, their frequency spectra are in principle of infinite extent. Thus one should have access to different portions of the signal's frequency spectrum through the measurement process. In particular, one can design a receiver system that differentiates the received signal and hence has access to a higher portion of the beam's spectrum even though there is little energy radiated in that portion of the frequency spectrum. The intensity and energy of

the received signal are related to the higher-order correlation properties of the signals used to drive the aperture. As described in Refs. 3 and 5, since these higher-order correlation properties of the beam's signals involve the higher portions of the frequency spectra, diffraction affects them more slowly. Thus the diffraction lengths and rates of beam spread differ between the radiated and measured beam fields.

A derivative receiver is readily achieved in principle. A dipole whose length is shorter than the wavelengths of interest in the pulse, $k_{\max}L \leq 1$, will differentiate the signals it receives. Such a system has been realized with optoelectronic techniques, and the expected enhancements have been observed.[6-9] The photoconductive switches are excited with a Gaussian space–time laser beam, and the currents in the photoconductive region obtain a skewed Gaussian form. The receiving-system antennas can be designed to receive the radiated signal (one time derivative as in Section 3) or to differentiate the received signal (leading to the two-time-derivative behavior discussed below). Although these effects can be achieved with the optical-switch technology in the picosecond–terahertz region, it is not readily apparent what the corresponding system should be in the femtosecond–petahertz regime. Nonetheless, these systems should be available in the future and should result in the following beam-parameter enhancements. Note that these enhanced measured beam properties are readily accessible in the megahertz frequency region by using ultrasound beams in water, and they have been observed experimentally.[10,11] In fact, higher-derivative systems are possible in the ultrasound regime in which the transmitter and the receiver are time differentiators and lead to further enhancements.

The approximate signals measured by a derivative detector in the far field of the aperture can be readily derived from the corresponding expressions given in Section 3. In particular, let

$$\Lambda = \frac{1}{4p} + \left(\frac{w_0 r}{2cz}\right)^2. \tag{34}$$

One then can write

$$E_{\text{meas}}(r,\phi,z,t) \stackrel{\text{def}}{=} \partial_t E(r,\phi,z,t) \approx \frac{E_0}{\sqrt{p}}\frac{{w_0}^2}{8cz}\left[\frac{(z/c - t + r^2/2cz)^2 - 2\Lambda}{2\Lambda^{5/2}}\right] \times \exp\left[-\frac{(z/c - t + r^2/2cz)^2}{4\Lambda}\right]. \tag{35}$$

This leads to the far-field expressions

$$\mathcal{I}_{\max}^{\text{meas}}(r,\phi,z) = \frac{{E_0}^2}{p}\left(\frac{{w_0}^2}{8cz}\right)^2 \frac{4}{e^3}\Lambda^{-3}, \tag{36}$$

$$\mathcal{E}_{\text{meas}}(r,\phi,z) = \frac{{E_0}^2}{p}\left(\frac{{w_0}^2}{8cz}\right)^2 \frac{3\sqrt{2\pi}}{4}\Lambda^{-5/2}. \tag{37}$$

Therefore, as in the simple detector case, one can introduce[3,5] for this derivative-detector system the effective frequency ω_{meas} and the intensity quantity Υ_{meas}:

$${\omega_{\text{meas}}}^2 \stackrel{\text{def}}{=} \frac{\int_A dS' \int_{-\infty}^{\infty} dt\, |\partial_t{}^2 F(\mathbf{r}',t)|^2}{\int_A dS' \int_{-\infty}^{\infty} dt\, |\partial_t F(\mathbf{r}',t)|^2} = 3p = 3{\omega_{\text{rad}}}^2, \tag{38}$$

$$\Upsilon_{\text{meas}} \stackrel{\text{def}}{=} \frac{\max_t \int_A dS' |\partial_t{}^2 F(\mathbf{r}',t)|^2}{\int_A dS' \int_{-\infty}^{\infty} dt\, |\partial_t{}^2 F(\mathbf{r}',t)|^2} = \frac{32}{3e^3}\left(\frac{p}{2\pi}\right)^{1/2} = \frac{32}{3e^3\sqrt{2\pi}}\omega_{\text{rad}}. \tag{39}$$

Consequently, introducing the far-field ratios of the measured maximum intensity and measured energy in a plane orthogonal to the axis of propagation to their values on that axis, we find that

$$\Gamma_{\text{int},\perp}^{\text{meas}}(r,\phi,z) \stackrel{\text{def}}{=} \frac{\mathcal{I}_{\max}^{\text{meas}}(r,\phi,z)}{\mathcal{I}_{\max}^{\text{meas}}(r=0,\phi,z)} = \left(1 + p\frac{{w_0}^2 r^2}{c^2 z^2}\right)^{-3}, \tag{40}$$

$$\Gamma_{\text{enrg},\perp}^{\text{meas}}(r,\phi,z) \stackrel{\text{def}}{=} \frac{\mathcal{E}_{\text{meas}}(r,\phi,z)}{\mathcal{E}_{\text{meas}}(r=0,\phi,z)} = \left(1 + p\frac{{w_0}^2 r^2}{c^2 z^2}\right)^{-5/2}, \tag{41}$$

so that the rates of spread of the measured beam intensity and the measured energy in the far field are

$$\theta_{\text{int}}^{\text{meas}} \approx ({R_{\text{int}}}^{-1/3} - 1)^{1/2}\frac{\lambda_{\text{rad}}}{2\pi w_0}, \tag{42}$$

$$\theta_{\text{enrg}}^{\text{meas}} \approx ({R_{\text{enrg}}}^{-2/5} - 1)^{1/2}\frac{\lambda_{\text{rad}}}{2\pi w_0}, \tag{43}$$

respectively. In addition, by introducing the effective frequency ω_{rad} of the radiated spectrum as a normalization term for the additional time derivative (recall that ω_{rad} is naturally associated with the aperture transmission process; hence by reciprocity it should be associated with the reception process as well), the rates of the measured beam energy decay and the measured intensity decay in the far field can be defined and have the values

$$\tilde{\Gamma}_{\text{enrg},\parallel}^{\text{meas}}(r=0,\phi,z) \stackrel{\text{def}}{=} \frac{\mathcal{E}_{\text{meas}}(r=0,\phi,z)}{{\omega_{\text{rad}}}^2\mathcal{E}(r=0,\phi,z=0)} = \left(\frac{\omega_{\text{meas}}}{\omega_{\text{rad}}}\right)^2\left(\frac{L_{\text{rad}}}{z}\right)^2 \equiv \left(\frac{L_{\text{enrg}}^{\text{meas}}}{z}\right)^2, \tag{44}$$

$$\tilde{\Gamma}_{\text{int},\parallel}^{\text{meas}}(r=0,\phi,z) \stackrel{\text{def}}{=} \frac{\mathcal{I}_{\max}^{\text{meas}}(r=0,\phi,z)}{{\omega_{\text{rad}}}^3\mathcal{E}(r=0,\phi,z=0)} = \frac{\Upsilon_{\text{meas}}}{\omega_{\text{rad}}}\left(\frac{\omega_{\text{meas}}}{\omega_{\text{rad}}}\right)^2\left(\frac{L_{\text{rad}}}{z}\right)^2 \equiv \left(\frac{L_{\text{int}}^{\text{meas}}}{z}\right)^2, \tag{45}$$

where we have introduced the diffraction lengths associ-

ated with the measured field:

$$L_{\text{enrg}}^{\text{meas}} \overset{\text{def}}{=} \left(\frac{\omega_{\text{meas}}}{\omega_{\text{rad}}}\right) L_{\text{rad}}, \tag{46}$$

$$L_{\text{int}}^{\text{meas}} \overset{\text{def}}{=} \left(\frac{\Upsilon_{\text{meas}}}{\omega_{\text{rad}}}\right)^{1/2} \left(\frac{\omega_{\text{meas}}}{\omega_{\text{rad}}}\right) L_{\text{rad}}. \tag{47}$$

Comparisons of the measured beam parameters with those associated with the radiated beam or the corresponding cw beam reveal significant differences. In particular, taking the $1/e$ roll-off point for the beam spread, one has

$$L_{\text{enrg}}^{\text{meas}} = 1.73 L_{\text{rad}} = 1.73 L_{\text{cw}}, \tag{48}$$

$$L_{\text{int}}^{\text{meas}} = 0.797 L_{\text{rad}} = 0.797 L_{\text{cw}}, \tag{49}$$

$$\theta_{\text{int}}^{\text{meas}} = 0.780 \theta_{\text{int}}^{\text{rad}} = 0.444 \theta_{\text{int}}^{\text{cw}}, \tag{50}$$

$$\theta_{\text{enrg}}^{\text{meas}} = 0.718 \theta_{\text{enrg}}^{\text{rad}} = 0.496 \theta_{\text{enrg}}^{\text{cw}}. \tag{51}$$

Thus we find that the diffraction length for the measured beam energy is 1.73 times that of the corresponding cw beam energy or intensity diffraction lengths and is 2.17 times the diffraction length for the measured beam intensity. Since $\omega_{\text{meas}}/\omega_{\text{rad}} = \sqrt{3.0}$, Eq. (44) indicates that the measured beam energy is three times the corresponding cw beam energy in the far field of the aperture. Similarly, since $\Upsilon_{\text{meas}}/\omega_{\text{rad}} = 0.212$, Eq. (45) indicates that the maximum intensity is 0.636 times the cw value. On the other hand, the beam spread for the measured beam energy is 0.496 times the corresponding cw beam energy spread, but it is 1.12 times the beam spread for the measured beam intensity. These results for the measured beam intensity and energy seem contradictory, but they are not for this case. One must recall that the intensity quantities are taken as the maxima over time, so an energylike conservation argument will not hold for them. Most of the cases treated to date have dealt with signals and their derivatives that have significant differences between them and that, as a consequence, have shown significant enhancements simultaneously in both the measured beam intensity and energy. Note that, as shown in Ref. 5, the measured beam energy does satisfy a generalized antenna theorem (see, for instance, Ref. 2, p. 672); i.e., if $A_{1/e} = \pi w_0^2/2$ is the effective source aperture area and $\pi(\theta_{\text{enrg}}^{\text{meas}})^2$ is the effective far-field solid angle, where $\theta_{\text{enrg}}^{\text{meas}}$ must now be measured at the $1/e^2$ point of the energy profile, then their product yields

$$A_{1/e} \times \pi(\theta_{\text{enrg}}^{\text{meas}})^2 = \frac{\pi^2 w_0^2}{2}(R_{\text{int}}^{-1/3} - 1)\left(\frac{\lambda_{\text{rad}}}{2\pi w_0}\right)^2 = \frac{9(e^{2/3} - 1)}{8}\lambda_{\text{meas}}^2 = 1.07\lambda_{\text{meas}}^2 \approx \lambda_{\text{meas}}^2. \tag{52}$$

Thus the smaller measured beam spread is intimately connected with the smaller effective wavelength.

Therefore the measured pulsed Gaussian beam has properties quite distinct from but analogous to the radiated pulsed Gaussian beam. As explained in Refs. 3 and 5, these differences can be associated with the differences in the rates of diffraction of the higher-order correlation properties of the beams. Since they are associated with higher portions of the frequency spectra that are present in the time-limited signals, those higher-order moments have different diffraction lengths and rates of beam spread, as evidenced above, which are accessible through derivative-detection processes. The enhancement of the measured beam properties over those of the radiated field is summarized in Fig. 1. Note that this pulsed Gaussian beam example is one of the simplest cases that reveals these enhanced beam properties, but, as emphasized in Refs. 3 and 5, the signals used to drive an aperture or array can be designed to increase the magnitudes of these enhancements substantially.

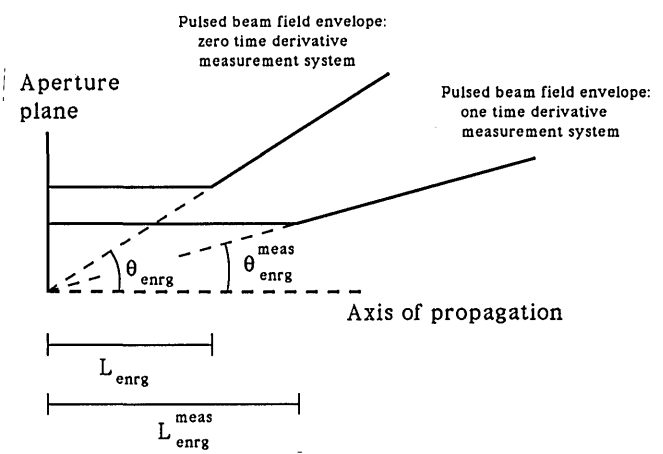

Fig. 1. Energy-distribution envelopes. Diffraction affects the higher-order coherence properties of a beam generated by an ultrawide-bandwidth pulse-driven aperture more slowly than it affects the lower-order coherence properties. The envelopes of the energy distribution in a pulsed beam are defined by their diffraction lengths and the rate of spread of the beam in the region beyond their diffraction lengths.

5. NUMERICAL SIMULATIONS

The situation that we have modeled in Section 3 could occur, at least to a first-order approximation, when an optical fiber is terminated and a linearly polarized, Gaussian space–time pulse that is traveling in this waveguide is launched into free space. We choose for discussion purposes the parameter values $w_0 = 2.5$ μm, $a = 5.0$ μm, and $p = 1.90 \times 10^{30}$. These values correspond to launching a Gaussian pulse from a fiber-optic waveguide whose core radius is 5.0 μm. This pulse has a 1.45-fs full width between its $1/e$ amplitude points; its Fourier spectrum has a $1/e$ roll-off point at the frequency $f_{1/e} = 4.39 \times 10^{14}$ Hz, or radian frequency $\omega_{1/e} = 2.76 \times 10^{15}$ rad/s, which corresponds to the wavelength $\lambda_{1/e} = 0.683$ μm. The pulse has a maximum amplitude of 0.018 at $r = 5.0$ μm, the edge of the aperture, which is small enough for our purposes here. No other aspects of the fiber need be considered. The initial pulse's time history is plotted versus time in Fig. 2, and its Fourier spectrum is plotted versus radian frequency in Fig. 3. The effective frequency of this pulse is $f_{\text{rad}} = 2.19 \times 10^{14}$ Hz, or $\omega_{\text{rad}} = 1.38 \times 10^{15}$ rad/s, which corresponds to the wavelength $\lambda_{\text{rad}} = 1.367$ μm. An analogous situation, but scaled down to terahertz frequencies, arises in the large-aperture photoconductive-switch picosecond–terahertz sources.[12–14]

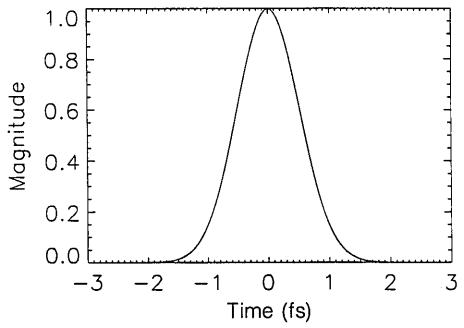

Fig. 2. Time history of the initial Gaussian pulse.

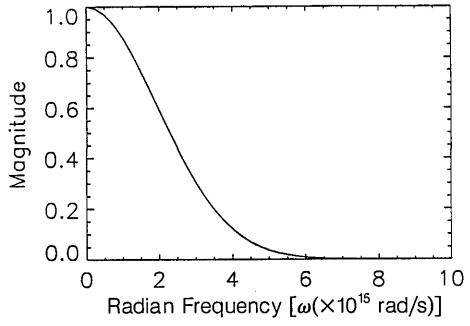

Fig. 3. Fourier spectrum of the initial Gaussian pulse.

We have developed a numerical simulator to calculate Eq. (9) directly to check our predictions. The waves that are generated by the simulator are visualized with PV-WAVE, a commercial software system for plotting and displaying images. Equation (9) is also implemented by using the prepackaged fast-Fourier-transform (FFT) routine provided with PV-WAVE. The FFT routine is used in two places within the program. It is used first to produce a spectrum of the initial driving pulse F and is used again to calculate the inverse Fourier transform in Eq. (9). This approach makes the program more versatile since it allows for an arbitrary driving pulse.

A systematic numerical investigation was undertaken with the simulator to study the evolution of the pulsed Gaussian beam as it propagates away from the initial aperture, i.e., as time (or distance) increases. Several standard sampling criteria on the window size T and the number of time samples N associated with FFT routines were readily met with the values $T = 25$ fs and $N = 512$ samples.

Contour plots of the Gaussian pulse beam field that were created with our simulator are shown in Fig. 4. Each plot was generated by constructing the time signals received at a set of radial positions in a plane perpendicular to the propagation axis at a specified distance from the initial aperture. There are 32 radial positions in each plot; this was the minimum number of radial time signals needed to produce a smooth surface plot. The total radial distance in each plot is 7.5 μm, and the total time record is 25.0 fs. The distances from the aperture represented by Figs. 4(a), 4(b), 4(c), and 4(d) are, respectively, 15.0, 30.0, 45.0, and 60.0 μm. Because the axial coordinate is fixed and the wave is calculated in time, the image is reversed from what one might expect. The form of these pictures is analogous to what a detector array would see if it were placed in a plane perpendicular to the axis of propagation and sampled the pulsed beam as it went by.

The time-derivative behavior expected from relation (14) is apparent in the figures; the pulse is completely

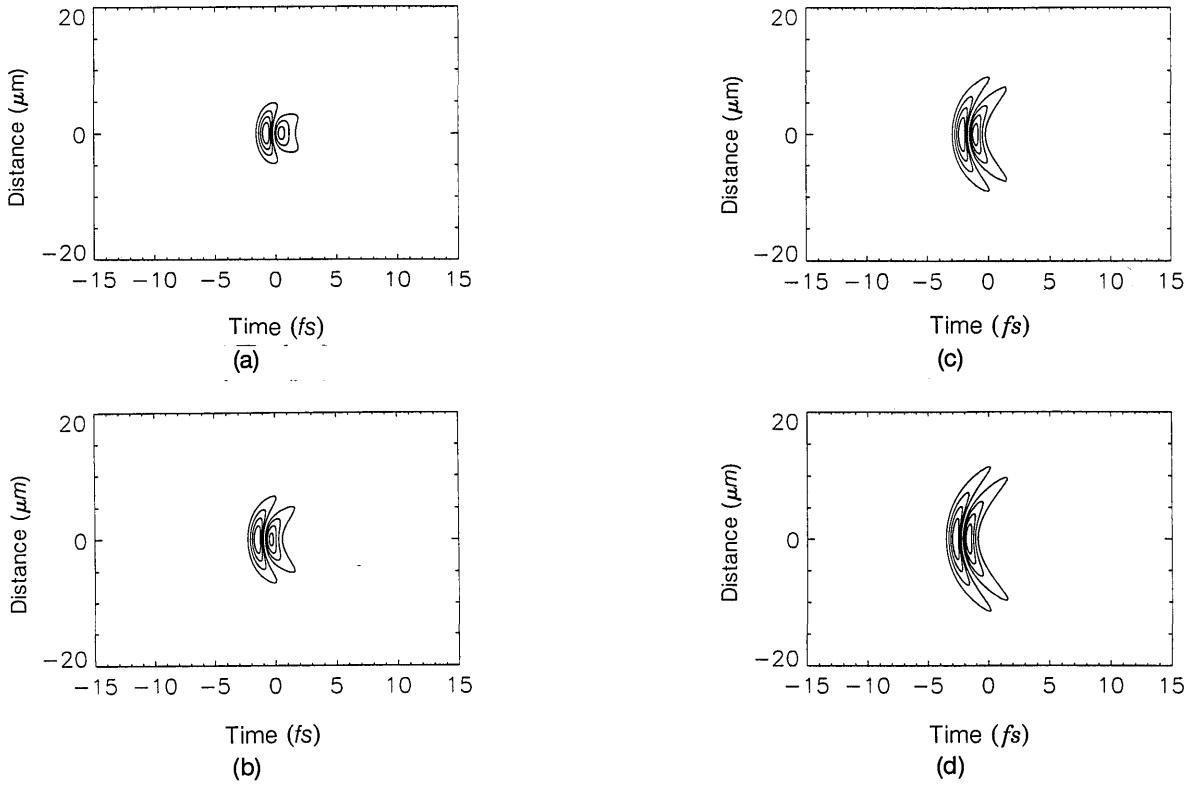

Fig. 4. Contour map of the pulsed Gaussian beam field as observed in the planes (a) $z = 15.0$ μm, (b) $z = 30.0$ μm, (c) $z = 45.0$ μm, and (d) $z = 60.0$ μm. The transverse distance from the propagation axis is given along the vertical axis.

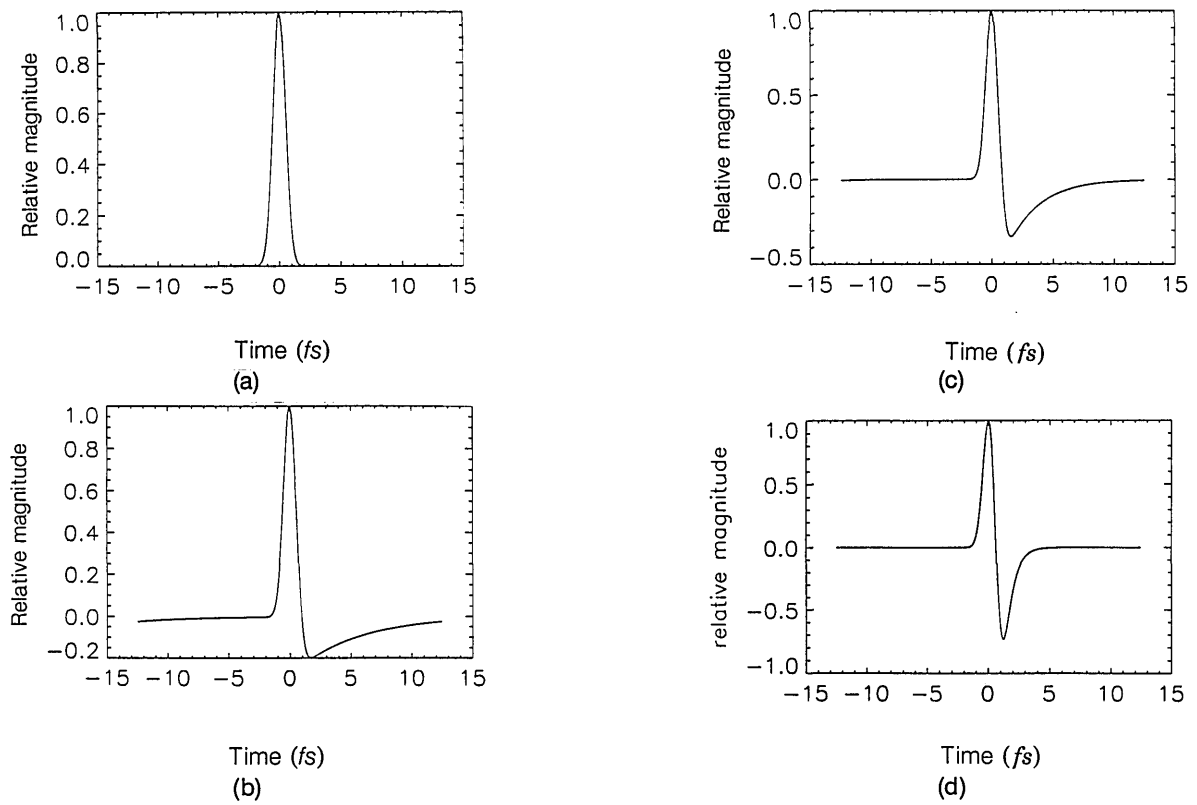

Fig. 5. Pulsed Gaussian beam's time signals along the propagation axis at distances (a) $z = 0.0$ μm, (b) $z = 2.0$ μm, (c) $z = 4.0$ μm, and (d) $z = 16.0$ μm. As the field propagates from the initial aperture, it evolves into a time derivative of the initial field.

in the far field in Fig. 4 ($L_{rad} = 14.36$ μm). For clearer illustration of this behavior, the on-axis signal $E(r = 0, \phi, z, t)$ is graphed versus time in Figs. 5(a), 5(b), 5(c), and 5(d) for the z locations $z = 0.0$, 2.0, 4.0, and 16.0 μm, respectively. This sequence clearly demonstrates the evolution of the initial Gaussian pulse into its first-derivative form as the beam propagates farther from the aperture.

The results of relation (7) for the cw beam energy and intensity spreads at the cw frequency $\omega_{cw} = \omega_{rad}$ are plotted in Fig. 6. Recall that the initial waist (distance from the core centerline to the 1/e field magnitude) is 2.5 μm. The 1/e beam-spread curves for the intensity and energy of the pulsed Gaussian beam obtained directly from Eq. (9) are given (solid curves) in Figs. 7 and 8, respectively.

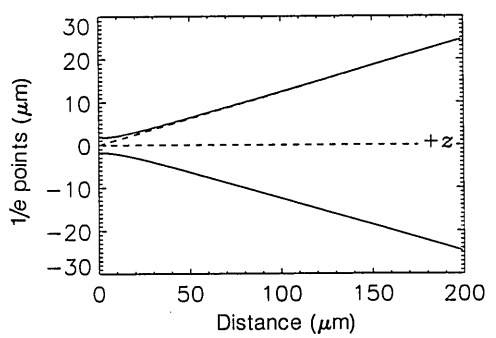

Fig. 6. Intensity and energy profiles of the cw Gaussian beam (solid curve) versus distance along the direction of propagation. The rate of spread of the intensity and energy are identical. The cw frequency is $f = f_{rad} = 2.19 \times 10^{14}$ Hz, and the initial waist of the Gaussian amplitude taper is $w_0 = 2.5$ μm. The oblique dashed line represents the asymptote given by relation (7).

Similarly, the 1/e beam-spread curves for the intensity and energy of the pulsed Gaussian beam predicted from Eqs. (22′) and (27′) are shown in Figs. 9 and 10 (dotted–dashed curves), respectively. They begin at $z = 50.0$ μm, well into the far field. The solid curves in Figs. 9 and 10 are the beam-spread curves of the corresponding cw Gaussian beam. Asymptotes to the numerically obtained curves in Figs. 7 and 8 allow us to calculate accurately the pulsed Gaussian beam-spread rates. We find from Figs. 7 and 8 the values $\theta_{int} = 4.04°$ and $\theta_{enrg} = 4.84°$. The predicted values are, respectively, 4.02° and 4.87°. The agreement improves for larger distances away from the aperture. Comparing Fig. 6 with Figs. 7–10, one sees that the pulsed Gaussian beam diffracts more slowly than the corresponding cw beam.

Figure 11 shows the values of the pulsed beam's maximum intensity and energy in the plane $z = 200.0$ μm. As indicated by a comparison of Eqs. (21) and (26), the profile of the maximum intensity of the pulsed beam is narrower than the corresponding beam-energy profile.

The pulsed Gaussian field measured with a one-time-derivative receiver at $z = 45.0$ μm is depicted in Fig. 12. This figure corresponds to the radiated field shown in Fig. 4(c). The appearance of the additional amplitude peak results from the two-time-derivative behavior exhibited by relation (35). The associated measured beam-intensity and energy spread (dotted–dashed) curves are included, respectively, in Figs. 7 and 8. Similarly, the 1/e beam-spread curves for the intensity and energy profiles of the pulsed Gaussian beam predicted from relations (42) and (43) are shown (triple-dotted–dashed curves), respectively, in Figs. 9 and 10. Comparing Figs. 6–10, one sees

that the higher-order-derivative properties of the pulsed Gaussian beam diffract more slowly than those associated with the corresponding cw beam or lower-order-derivative pulsed Gaussian beam fields. The enhancements that would be obtained with a time-derivative measurement system (receiver) are apparent.

6. CONCLUSIONS

The near- and far-field behaviors of a pulsed Gaussian beam were derived analytically and were supported with numerical simulations. In particular, expressions were given for the rates of decay and spread of this pulsed beam's intensity and energy. The expected translational behavior of the beam near the initial aperture and the expected time-derivative behavior of the beam field far from it were recovered. It was shown that the rates of decay or spread of the intensity and energy profiles are different, in contrast to the corresponding cw Gaussian beam case. It was also shown that the pulsed Gaussian beam's intensity profile is narrower than its energy profile. These effects are further enhanced if the beam field is measured with a time-derivative system. The corresponding two-derivative beam-field expressions were derived. All the relations agreed with the general pulsed-beam results given in Ref. 3.

These single- and higher-order-derivative pulsed-beam results have been confirmed with ultrasound experiments in water.[10,11] The given results are testable experimentally in the terahertz regime by using photoconductive switch technology. Similar experimental tests may soon be available in the petahertz regime as ultrawide-bandwidth supercontinuum light sources are further developed. The present results indicate that care must be exercised when pulsed beams are considered, particularly when questions concerning the roles of intensity (point) and energy (average) effects are raised. The differences

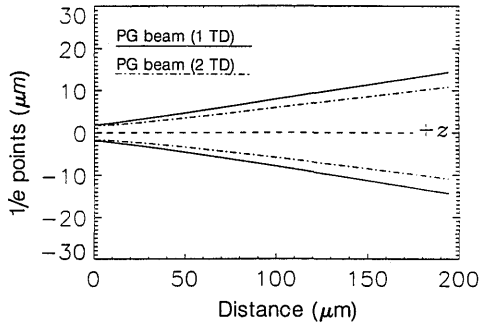

Fig. 7. Rates of spread of the pulsed Gaussian (PG) beam's maximum-intensity profile for the one-time-derivative (1TD) and two-time-derivative (2TD) systems versus distance along the direction of propagation. These curves are obtained directly from numerical simulations of the beam fields defined by Eq. (9) and its time derivative.

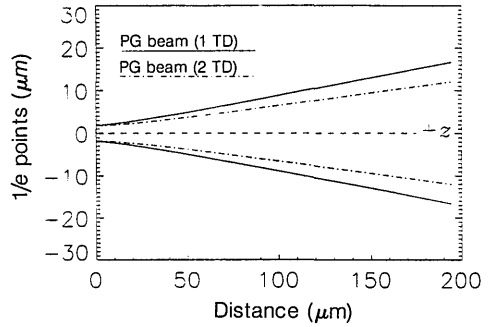

Fig. 8. Rates of spread of the pulsed Gaussian (PG) beam's energy profile for the one-time-derivative (1TD) and two-time-derivative (2TD) systems versus distance along the direction of propagation. These curves are obtained directly from numerical simulations of the beam fields defined by Eq. (9) and its time derivative.

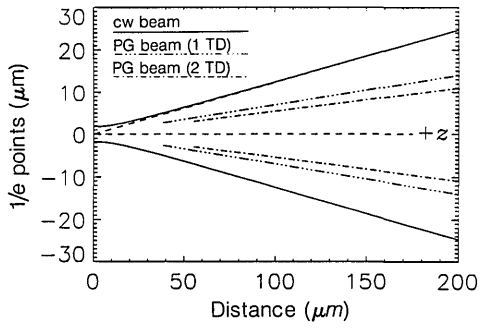

Fig. 9. Maximum-intensity profile of various beams versus distance along the direction of propagation. The rate of spread in the far field of the maximum intensity is generated with Eq. (22′) for the one-time-derivative (1TD) pulsed Gaussian (PG) beam field and with relation (42) for the two-time-derivative (2TD) pulsed Gaussian beam field. The solid curves represent the beam-spread values for the corresponding cw Gaussian field with $\omega_{cw} = \omega_{rad}$. The dashed line represents the asymptote to the cw curve.

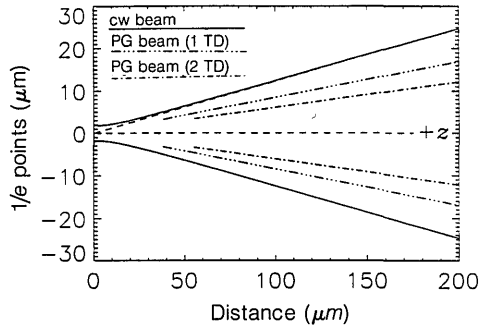

Fig. 10. Energy profile of various beams versus distance along the direction of propagation. The rate of spread in the far field of the energy is generated with Eq. (27′) for the one-time-derivative (1TD) pulsed Gaussian (PG) beam field and with relation (43) for the two-time-derivative (2TD) pulsed Gaussian beam field. The solid curves represent the beam-spread values for the corresponding cw Gaussian field with $\omega_{cw} = \omega_{rad}$. The dashed line represents the asymptote to the cw curve.

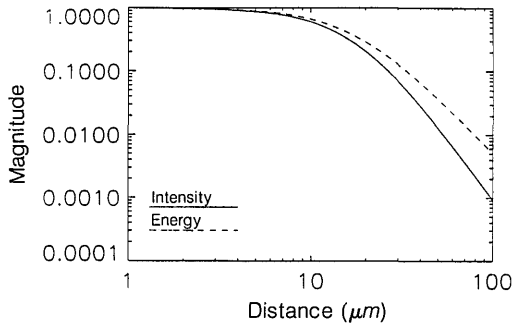

Fig. 11. Intensity and energy profiles of the pulsed Gaussian beam in the plane $z = 200.0$ μm. Both profiles have been normalized to unity.

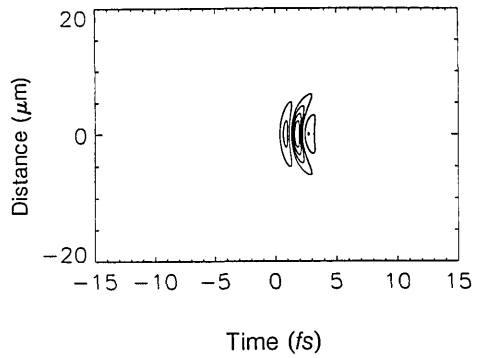

Fig. 12. Contour map of the pulsed Gaussian beam field measured in the plane $z = 45.0$ μm with a one-time-derivative receiving (measurement) system. The transverse distance from the propagation axis is given along the vertical axis.

between the intensity of the pulsed beam and the energy delivered by it to a target must be taken into account during the design and analysis of any experimental investigation.

ACKNOWLEDGMENTS

This work was supported in part by the Lawrence Livermore National Laboratory under the auspices of the U.S. Department of Energy under contract W-7405-ENG-48.

REFERENCES

1. A. Yariv, *Quantum Electronics*, 3rd ed. (Wiley, New York, 1989).
2. A. Siegman, *Lasers* (University Science, Mill Valley, Calif., 1986).
3. R. W. Ziolkowski, "Localized wave physics and engineering," Phys. Rev. A **44,** 3960–3984 (1991).
4. I. S. Gradshteyn and I. M. Ryzhik, *Table of Integrals, Series, and Products* (Academic, New York, 1980).
5. R. W. Ziolkowski, "Properties of electromagnetic beams generated by ultra-wide bandwidth pulse-driven arrays," IEEE Trans. Antennas Propag. **40,** 888–905 (1992).
6. M. van Exeter and D. R. Grischkowsky, "Characterization of an optoelectronic terahertz beam system," IEEE Trans. Microwave Theory Tech. **38,** 1684–1691 (1990).
7. M. van Exeter, Ch. Fattinger, and D. R. Grischkowsky, "High-brightness terahertz beams characterized with an ultrafast detector," Appl. Phys. Lett. **55,** 337–339 (1989).
8. Y. Pastol, G. Arjavalingam, J.-M. Halbout, and G. V. Kopcsay, "Coherent broadband microwave spectroscopy using picosecond optoelectronic antennas," Appl. Phys. Lett. **54,** 307–309 (1989).
9. C. R. Lutz and A. P. deFonzo, "Far-field characteristics of optically pulsed millimeter wave antennas," Appl. Phys. Lett. **54,** 2186–2188 (1989).
10. R. W. Ziolkowski, D. K. Lewis, and B. D. Cook, "Evidence of localized wave transmission," Phys. Rev. Lett. **62,** 147–150 (1989).
11. R. W. Ziolkowski and D. K. Lewis, "Verification of the localized-wave transmission effect," J. Appl. Phys. **68,** 6083–6086 (1990).
12. X.-C. Zhang, B. B. Hu, J. T. Darrow, and D. H. Auston, "Generation of femtosecond electromagnetic pulses from semiconductor surfaces," Appl. Phys. Lett. **56,** 1011–1013 (1990).
13. X.-C. Zhang, J. T. Darrow, B. B. Hu, D. H. Auston, M. T. Schmidt, P. Tham, and E. S. Yang, "Optically induced electromagnetic radiation from semiconductor surfaces," Appl. Phys. Lett. **56,** 2228–2230 (1990).
14. N. Froberg, M. Mack, B. B. Hu, X.-C. Zhang, and D. H. Auston, "500 GHz electrically steerable photoconducting antenna array," Appl. Phys. Lett. **58,** 446–448 (1991).